Concentrations, sources, and influential factors of water-soluble ions of atmospheric particles in Dunhuang Mogao Grottoes, a world heritage site in China

YANG Xiaoju[1,2,3,4], WU Fasi[1,2], XU Ruihong[1,2], LI Na[5], ZHANG Zhengmo[1,2], XUE Ping[1,2], WANG Wanfu[1,2], ZHAO Xueyong[3*]

[1] National Research Center for Conservation of Ancient Wall Paintings and Earthen Sites, Dunhuang Academy, Dunhuang 736200, China;
[2] Gansu Provincial Research Center for Conservation of Dunhang Cultural Heritage, Dunhuang 736200, China;
[3] Naiman Desertification Research Station/Urat Desert-Grassland Research Station, Northwest Institute of Eco-Environment and Resources, Chinese Academy of Sciences, Lanzhou 730000, China;
[4] University of Chinese Academy of Sciences, Beijing 100049, China;
[5] Chinese Academy of Cultural Heritage, Beijing 100049, China

Abstract: Atmospheric particle pollution is one of the major factors leading to degradation of ancient wall paintings, particularly heritage sites in arid and semi-arid regions. However, current systematic research on the changes, sources, and influential factors of atmospheric particulate matter and its water-soluble ion concentrations is not sufficient. Thus, the major water-soluble ion concentrations, sources, and influential factors of atmospheric particles $PM_{2.5}$ and PM_{10} (particulate matter with an aerodynamic equivalent diameter ≤2.5 and 10.0 μm, respectively, in ambient air) were collected from Cave 16 and its ambient exterior environment in the Dunhuang Mogao Grottoes, China, between April 2015 and March 2016. Results showed that the concentrations of $PM_{2.5}$ and PM_{10} inside and outside the cave were the highest in March 2016 and the lowest in December 2015. The higher particle concentration from March to May was related to the frequent occurrence of sand and dust events, and the lower particle concentration from June to September was associated with good diffusion conditions, increased precipitation, and an established cave shelterbelt. The concentration of particulate matter inside the cave was affected by the concentration of particles in the air outside the cave. Ca^{2+}, NH_4^+, Na^+, Cl^-, and SO_4^{2-} were the main components of the total ions of $PM_{2.5}$ and PM_{10} both inside and outside the cave. The total ions inside the cave were frequently affected by the disturbance of tourists' activities during the peak tourist season from May to August. Under the influence of dust, the total concentrations of Cl^-, SO_4^{2-}, Na^+, NH_4^+, and Ca^{2+} in particles of different sizes inside and outside the cave increased, and the concentrations of Cl^-, SO_4^{2-}, Na^+, and Ca^{2+} decreased during precipitation period. Backward air mass trajectory analysis suggested that the pollutants were mainly from Xinjiang, China. The pollutant sources of air particulates are straw burning, secondary pollution sources, soil dust, dry spring rivers, and tourist activities.

Keywords: grotto temple; atmospheric particulate matter pollution; water-soluble ion; water and salt transport; heritage preventive conservation

Citation: YANG Xiaoju, WU Fasi, XU Ruihong, LI Na, ZHANG Zhengmo, XUE Ping, WANG Wanfu, ZHAO Xueyong. 2022. Concentrations, sources, and influential factors of water-soluble ions of atmospheric particles in Dunhuang Mogao Grottoes, a world heritage site in China. Journal of Arid Land, 14(12): 1395–1412. https://doi.org/10.1007/s40333-022-0036-6

*Corresponding author: ZHAO Xueyong (E-mail: zhaoxy@lzb.ac.cn)
Received 2022-06-26; revised 2022-10-27; accepted 2022-11-10

1 Introduction

Cultural heritage is the common wealth of humankind, and climate change, natural disasters, environmental pollution, and unreasonable management have caused serious damage to heritage conservation (Abbott, 2010; Li et al., 2013; Merello et al., 2014; Chatoutsidou et al., 2015; Vidal et al., 2019; Sakka et al., 2020; Ogura et al., 2021). Air particulates have a significant impact on global and regional climate change and environmental systems (Bouchlaghem et al., 2009; Guan et al., 2017; Yao et al., 2019), and damage cultural relics through coverage pollution and chemical corrosion (Pipal et al., 2014; Uring et al., 2019; Zhang et al., 2022). The deposition of atmospheric particulates on the surface of cultural relics change the color and texture of these relics, and affect their aesthetic value and visual effects (Brimblecombe, 1990; Natarajan et al., 2022), and certain chemicals in the dust will also affect murals and painted sculptures. The acidic components, such as sulfate, nitrate, and other small molecular organic acids, react with mineral pigments in the painted layers during the process of spreading and sedimentation. Long-term accumulation will cause corrosion and damage to cultural relics in caves (Hanapia and Din, 2012; Ogura et al., 2021), and the carbon and acid components will also react with $CaCO_3$ to form a black or grey crust, which will further corrode the pigment layer (Ghedini et al., 2000; Sabbioni et al., 2003). The process of cleaning particles will cause further mechanical wear. Numerical simulations conducted by Tétreault (2003) showed that for the preservation of cultural relics for 100 a, the maximum allowable concentration of $PM_{2.5}$ should be limited to 0.1 μg/m^3. Under the environmental conditions of $PM_{2.5}$ of 10.0 μg/m^3, the time of nondestructive preservation of cultural relics is only 1 a.

As early as the middle of the 19th century, the National Gallery of England had already begun to study the corrosive effects of the inside atmosphere on cultural relics (Broughton et al., 1875). Ghedini et al. (2011) analyzed the composition of water-soluble ions in atmospheric particulate matter surrounding the buildings of the Florence Cathedral. Singh and Sharma (2012) studied the seasonal changes and sources of PM_{10} in the Taj Mahal in India, and found that PM_{10} had an obvious seasonal change, and its source was mainly soil crust, vehicle, and industrial emissions. Chinese scientists conducted comprehensive monitoring and researches on inside and outside air quality in the Emperor Qin Shihuang's Mausoleum, Terra-cotta Warriors, Horses Museum, Exhibition Hall Museum, and the Jinsha Site Museum, and it was found that water-soluble components have caused long-term harm to cultural relics (Cao et al., 2005; Hu et al., 2009; Li et al., 2019; Deng et al., 2022).

Ancient murals are important components of cultural relics. The Dunhuang Mogao Grottoes (40°05′17″N, 94°40′16″E; 1334 m a.s.l.), famous for their ancient murals, are situated at the western end of the Hexi Corridor of the Gansu Province, northwestern China. The Mogao Grottoes, which comprise of 492 caves, 45×10^3 m^2 of murals, and 2400 painted sculptures (Fan, 2000), was designated as a World Heritage Site by UNESCO (United Nations Educational, Scientific and Cultural Organization) in 1987 (Agnew, 2004). Because of its location on the southeastern edge of the Kumtag Desert and the eastern foot of the Mingsha Mountain, the dry climate provides unique natural conditions for the long-term preservation of the murals. The study area has a strong northwesterly and southwesterly wind, and a large amount of sand is transported to the caves, even into the caves, causing serious harm to the murals outside and inside the caves (Wang, 2018). Sand particles carried by the southeasterly wind with high velocity may contribute to the deterioration of the paintings on the eastern wall of the Mogao Grotto Cave 285 (Mikayama et al., 2015). The windblown sand causes the murals to undergo detachment and flaking (Ogura et al., 2021). Small air particles with a large specific surface area easily carry heavy metals, acidic oxides, organic pollutants, and microorganisms (Poulain et al., 2021). When the humidity is high, a shell-like coating readily forms on the surface of cultural relics. Small particles enter the gaps of the murals, speeding up the flaking of the murals. When visitors come into the caves, the air currents in the caves change (Wang et al., 2016), and the air particles in the caves will repeatedly settle and adsorb on the surface of the cultural relics, leading to aggravation of the mural coverage

and health of tourists and staff.

At present, the research on atmospheric particulate matter pollution in the Mogao Grottoes mainly focuses on microbes, elements, organic carbon, and water-soluble ions (Wang et al., 2011; He et al., 2020; Xu et al., 2020; Yang et al., 2021). This study addresses the current situation of atmospheric particulate matter pollution in the Mogao Grottoes based on an analysis of the temporal and spatial changes in particulate matter and its water-soluble ions, the characteristics of atmospheric particulate matter concentration, water-soluble ions under extreme conditions (precipitation and sandstorms), and changes in water-soluble ions. Moreover, through the analysis of the airflow backward trajectory, we speculated the source of atmospheric pollutants in the Mogao Grottoes in the dusty weather, and the changes in the concentrations of atmospheric particles and their water-soluble ions inside and outside the Mogao Grottoes. We systematically and comprehensively analyzed their sources and influential factors, based on the following questions: (1) what are the differences in particle changes inside and outside the caves? (2) what is the source of water-soluble ions in atmospheric particles? and (3) what are the effects of natural factors and visitors' activities? The results are expected to provide important information for the control and treatment of air pollution in the Mogao Grottoes, and provide a reference for building a monitoring and early warning system for cultural relic protection and tourism opening decision-making.

2 Materials and methods

2.1 Study area

The Mogao Grottoes are 25 km from the Dunhuang City, surrounded by the Gobi area and river systems. The sampled sites were located in front of Cave 72 (outside the cave) and in Cave 16 (inside the open cave), which is 1 km west of the Daquan River, and the Kumtag Desert is located to the east (Fig. 1). The climate is extremely arid, with average annual precipitation of 39 mm, of which more than 59% is concentrated mainly from June to August. The annual relative humidity is 31%, the annual average temperature is 11.2℃, and the annual evaporation is about 4348 mm (Liu et al., 2020).

Fig. 1 Location of the sampling sites and air particulate pollution at the Dunhuang Mogao Grottoes. (a), aerial photo of the study area; (b), sandstorm pollution outside the cave; (c), dust reduction on the surface of sculptures inside the cave; (d), orthophoto of the Dunhuang Mogao Grottoes; (e), air particulate matter pollution inside the cave; (f), sampling point outside the cave; (g), sampling point inside the cave.

2.2 Plane section and air exchange rate of the cave

During the sampling period, the total number of tourists in the Mogao Grottoes was 1,147,735, and the monthly average number of tourists from April to December 2015 was 36,920, 66,065, 101,503, 216,793, 283,197, 168,084, 202,511, 22,699, and 8275, respectively. From January to March 2016, the monthly average number of tourists was 7605, 17,275, and 16,808, respectively.

When there are no tourists, the air exchange rate of small and medium-sized caves is generally less than 10 min. When there are tourists, the air exchange rate inside and outside the cave is correspondingly doubled, and the impact of tourists on the air exchange rate inside and outside the cave is obvious (Zhang et al., 2009).

The width of the door of Cave 16 is 4.0 m, the distance between cave door and tunnel is 7.5 m, and the distance between the entrance of tunnel and sampling instrument is 14.5 m. The cave door has screen windows, and the cave has wooden floors. There are three main ways for particles to enter the cave, i.e., infiltration, natural ventilation, and tourists (Fig. 2).

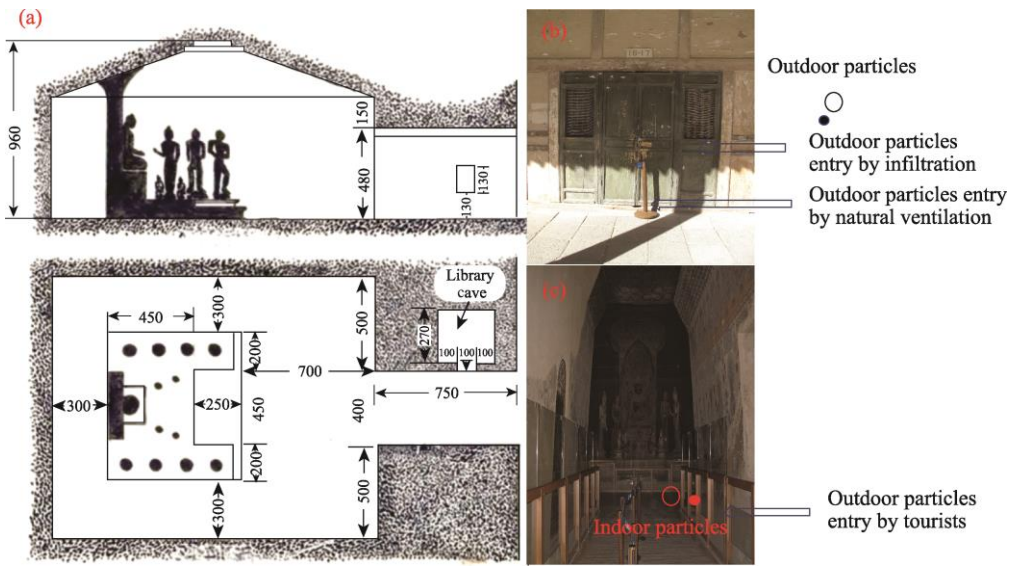

Fig. 2 Pathways of particles entering the cave. (a), hand drawing of Cave 16 of the Mogao Grottoes, 2004 (the measurement unit in the figure is cm); (b), wooden cave door; (c), inside the cave.

2.3 Air particulate matter data

$PM_{2.5}$ and PM_{10} samples were collected on quartz fiber filter papers (47 mm, Whatman, USA) by two parallel medium-volume air samplers (Dichotomous Partisol-Plus Model 2025, Thermo Scientific, USA) at each sampling site, at the flow rates of 15.00 and 1.67 L/min for 24 h, respectively, with separate samplings during dust and precipitation. At least 316 replicate samples were obtained from two sampling sites. To remove carbonaceous contaminants, we pre-heated the quartz filters at 500°C for 4 h in a muffle furnace before sampling. Before and after sampling, we equilibrated the filters for 24 h in a balance dish at a temperature of 20°C (±1)°C and a relative humidity of 50% (±5%). Before and after sampling, we weighed the weight of the filter membrane with electronic balance (AUY220, Shimadzu, Japan) three times. After sampling, we stored the filter membrane in a refrigerator below 0°C prior to weighing and water-soluble ion analysis.

2.4 Meteorological data

Air temperature, relative humidity, rainfall, wind speed, and wind direction were obtained from the weather station in front of Cave 72. These data in Gobi area were provided by the monitoring and early warning system platform of the Cave Monitoring Center of Dunhuang Academy.

2.5 Water-soluble ion sample preparation and detection

Major cations (Ca^{2+}, Mg^{2+}, Na^{+}, K^{+}, and NH_4^{+}) and major anions (F^{-}, Cl^{-}, NO_3^{-}, and SO_4^{2-}) of selected air particulate matter samples were measured using an ion chromatograph (Dionex-6000, Dionex, USA) (Li et al., 2016).

2.6 Quality assurance and control

All analytical procedures complied with strict quality assurance and control. The correlation coefficients of the standard working curves for the 9 water-soluble ions were all greater than 0.9990. All water-soluble ion concentrations had already been corrected by eliminating field blank values to eliminate the error caused by gas adsorption artifacts. The detection limit was 1 ng/mL, and the standard deviation was less than 5%. The determination limits for the ions were as follows: F^{-} (0.002 μg/m^3), Cl^{-} (0.001 μg/m^3), NO_3^{-} (0.004 μg/m^3), SO_4^{2-} (0.004 μg/m^3), Ca^{2+} (0.003 μg/m^3), Mg^{2+} (0.003 μg/m^3), Na^{+} (0.003 μg/m^3), K^{+} (0.006 μg/m^3), and NH_4^{+} (0.003 μg/m^3).

2.7 Statistical analysis

Statistical analysis was performed using SPSS v.22.0, and the graphs were drawn using Origin v.16.0. The Pearson method was used to analyze the correlations among air temperature, air pressure, relative humidity, wind speed, precipitation, number of tourists, and concentration of atmospheric particulate matter inside and outside the cave.

3 Results

3.1 Air particulate matter concentration

As shown in Figure 3, the monthly average concentrations of $PM_{2.5}$ and PM_{10} at the two monitoring points showed a similar trend, with a large monthly change. The concentrations of $PM_{2.5}$ and PM_{10} inside and outside the cave were both at the highest in March 2016 (339.4677, 421.6259, 708.2016, and 754.6400 μg/m^3) and the lowest in December 2015 (15.4841, 23.6697, 21.4576, and 27.7507 μg/m^3). Low concentrations of $PM_{2.5}$ and PM_{10} (variation ranges of $PM_{2.5}$ and PM_{10} inside the cave were 15.4841–49.5065 and 23.6697–74.0431 μg/m^3, respectively; variation ranges of $PM_{2.5}$ and PM_{10} outside the cave were 21.4576–113.8568 and 27.7507–132.8765 μg/m^3, respectively) were mainly concentrated from November 2015 to February 2016. The concentrations of $PM_{2.5}$ and PM_{10} inside the cave from June to September were different from those outside the cave (variation ranges of $PM_{2.5}$ and PM_{10} inside the cave were 49.8075–60.6085 and 70.0128–82.1617 μg/m^3, respectively; variation ranges of $PM_{2.5}$ and PM_{10} outside the cave were 58.7113–88.8595 and 69.1679–118.4600 μg/m^3, respectively).

$PM_{2.5}/PM_{10}$ ratios inside and outside the cave were both less than 1, indicating that the atmospheric particulate matter pollution of the Mogao Grottoes mainly came from coarse

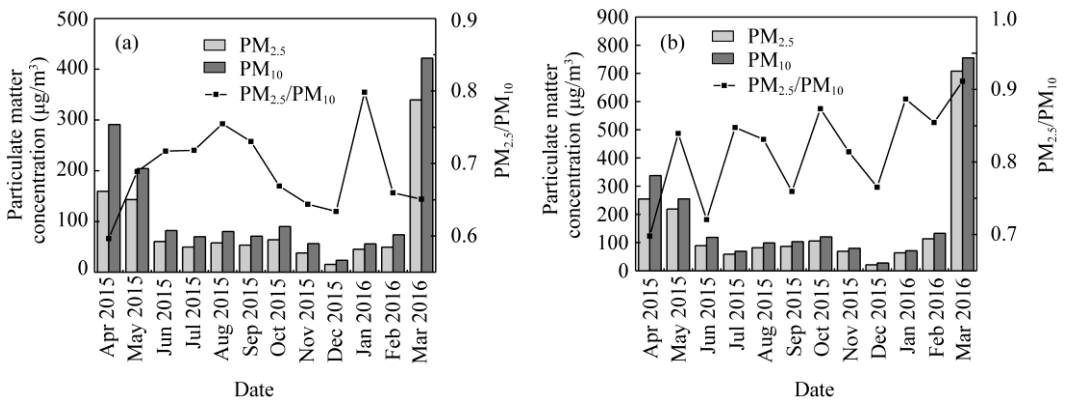

Fig. 3 Monthly variation of $PM_{2.5}$ and PM_{10} concentrations inside (a) and outside (b) the cave

particles with a diameter greater than PM_{10}. It is also clear that $PM_{2.5}/PM_{10}$ increased from the beginning to 15 August, and then decreased with a jump in January 2016 inside the cave, as well as a fluctuated increase outside the cave.

Correlation analysis revealed that $PM_{2.5}$ mass concentration inside the cave was significantly and positively correlated with that outside the cave (r=0.867, P<0.01), and the PM_{10} mass concentration was also significantly and positively correlated (r=0.903, P<0.01). This showed that the concentration of particulate matter in the cave was mainly affected by the concentration of particulate matter in the atmosphere outside the cave.

Table 1 showed the correlation analysis of $PM_{2.5}$ and PM_{10} concentrations inside and outside the cave with various meteorological elements and number of tourists. The concentrations of $PM_{2.5}$ and PM_{10} at the two sampling points were negatively correlated with air temperature, relative humidity, and precipitation. During the sampling period, the temperature outside and inside the cave varied from −16.66℃ to 40.71℃ and −3.36℃ to 23.00℃, respectively. The concentration of particulate matter inside the cave had a higher correlation with temperature than that of outside the cave. Temperature difference promotes air exchange. Annual precipitation of the Mogao Grottoes is 39 mm, concentrated in May–September. Concentrations of $PM_{2.5}$ and PM_{10} at the two sampling points were positively correlated with air pressure, wind speed, and number of tourists. The concentration of particulate matter in the cave had a strong correlation with number of tourists and wind speed, indicating that the number of tourists contributed more to the air pollution in the cave.

Table 1 Correlation coefficients of $PM_{2.5}$ and PM_{10} inside and outside the cave with meteorological factors and number of tourists

Sampling point	Air temperature	Relative humidity	Air pressure	Wind speed	Precipitation	Number of tourists
$PM_{2.5}$ outside	–0.164	–0.046	0.197	0.217	–0.382	0.586*
PM_{10} outside	–0.042	–0.123	0.107	0.299	–0.395	0.489
$PM_{2.5}$ inside	–0.191	–0.166	0.081	0.345	–0.271	0.615*
PM_{10} inside	–0.160	–0.192	0.083	0.377	–0.281	0.598*

Note: *, P<0.05 level.

3.2 Variation of water-soluble ions inside and outside the cave

3.2.1 Concentration of water-soluble ions

As shown in Table 2, the total concentrations of water-soluble ions in $PM_{2.5}$ and PM_{10} inside the cave were 11.0106 (±5.4744) and 22.3576 (±10.5183) μg/m^3, respectively, and the ion concentration was ranked as $Ca^{2+}>NH_4^+>Cl^->Na^+>SO_4^{2-}>K^+>NO_3^->Mg^{2+}>F^-$. Those outside the

Table 2 Concentrations of water-soluble ions of $PM_{2.5}$ and PM_{10} inside and outside the cave

Water-soluble ion	Inside the cave			Outside the cave		
	$PM_{2.5}$ (μg/m^3)	PM_{10} (μg/m^3)	$PM_{2.5}/PM_{10}$	$PM_{2.5}$ (μg/m^3)	PM_{10} (μg/m^3)	$PM_{2.5}/PM_{10}$
F^-	0.0244±0.0222	0.0406±0.0292	0.5651±0.1571	0.0121±0.0065	0.0236±0.0146	0.5488±0.1378
Cl^-	1.8148±1.1201	3.2967±1.9301	0.5640±0.1230	2.1414±1.8429	3.6763±2.5832	0.6117±0.1379
SO_4^{2-}	1.0807±1.1201	2.0888±1.7851	0.4883±0.1424	1.5293±2.1851	2.6484±2.7977	0.5498±0.1490
NO_3^-	0.4009±0.3349	0.7279±0.6338	0.5498±0.1041	0.5230±0.4101	0.8858±0.7251	0.6204±0.1027
Na^+	1.1287±0.8054	2.6107±1.7141	0.4496±0.1555	1.1014±0.7051	3.3736±3.8020	0.3935±0.1804
NH_4^+	1.8427±1.2874	2.9178±1.9891	0.6217±0.1770	1.6681±1.1033	2.7246±1.4897	0.5959±0.1633
K^+	0.4718±0.2525	0.9396±0.4702	0.5023±0.1133	0.4510±0.2507	0.9211±0.5518	0.4909±0.1009
Mg^{2+}	0.2946±0.2499	0.5676±0.3226	0.4759±0.1846	0.2397±0.1874	0.5367±0.3529	0.4288±0.1457
Ca^{2+}	3.9520±2.8727	9.1679±4.2838	0.4230±0.1907	4.0340±3.3046	10.5977±5.7177	0.3651±0.2167
TIC	11.0106±5.4744	22.3576±10.5183	-	11.7001±7.1713	25.3878±15.7937	-
NO_3^-/SO_4^{2-}	0.4206±0.2183	0.3471±0.1319	-	0.4420±0.2554	0.3617±0.1524	-

Note: TIC, total ion concentration. - means no value. Mean±SD.

cave were 11.7001 (±7.1713) and 25.3878 (±15.7937) μg/m, respectively, and ranked as Ca^{2+}>Cl^{-}>NH_4^+>SO_4^{2-}>Na^+>NO_3^->K^+>Mg^{2+}>F^-. The result showed that Ca^{2+}, NH_4^+, Na^+, Cl^-, and SO_4^{2-} were the main components of the total water-soluble ions of atmospheric air particulate matter both inside and outside the cave. The ratios of $PM_{2.5}/PM_{10}$ inside and outside the cave were 0.42–0.62 and 0.37–0.62, respectively, showing that 9 kinds of water-soluble ions were different in the degree of enrichment in particles of different sizes. The concentration of NH_4^+ in the fine particles inside the cave was relatively high, and the concentrations of Cl^-, NO_3^-, and NH_4^+ outside the cave were relatively high in the fine particulate matter.

It is clear that the ratio of each ion to total ion content was basically not changed, indicating that the composition of each ion was relatively stable, either inside or outside the cave (Fig. 4). The concentrations of Cl^- accounted for 16.48% and 14.76%, and 18.30% and 14.40%, of total water-soluble ions in $PM_{2.5}$ and PM_{10} inside and outside the cave, respectively. The concentrations of NH_4^+ accounted for 16.74% and 13.05%, and 14.26% and 10.73%, respectively, while the concentrations of Ca^{2+} accounted for 35.89% and 41.01%, and 34.48% and 41.74%, respectively.

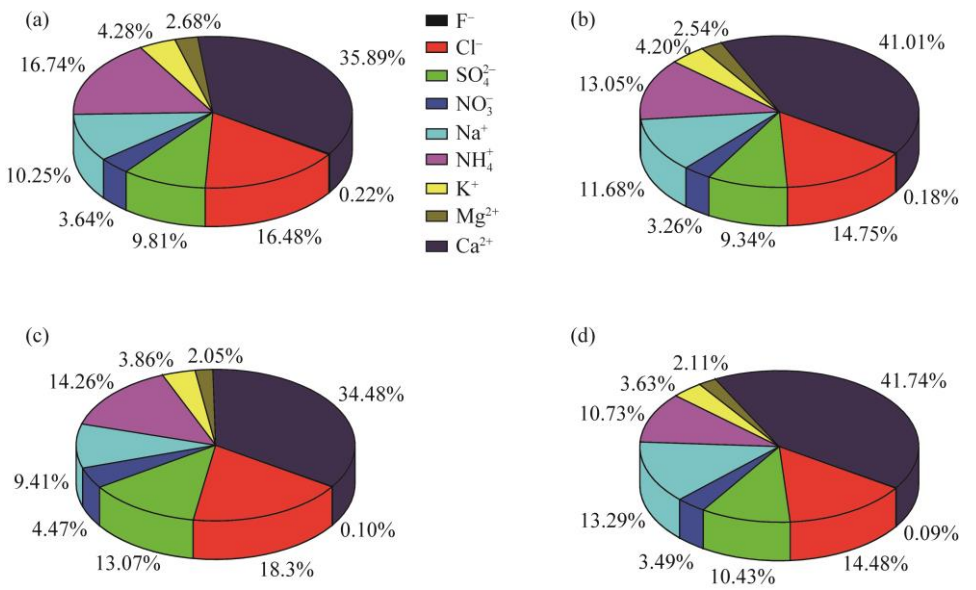

Fig. 4 Proportion of water-soluble ions in $PM_{2.5}$ (a) and PM_{10} (b) inside and outside (c and d) the cave

3.2.2 Monthly change of water-soluble ions

Figure 5 shows that the total ion concentration in $PM_{2.5}$ and PM_{10} in the cave, in general, increased in the year of measurement and fall to the lowest in September, and increased to peak or secondary peak in January or March. The concentrations of Cl^-, SO_4^{2-}, Na^+, K^+, Mg^{2+}, and Ca^{2+} increased from January to March 2016. The concentration of F^- was higher in July–August 2015, the concentration of NO_3^- was higher in November 2015–January 2016, and the concentration of NH_4^+ was higher in October 2015–January 2016.

Total ion concentration in $PM_{2.5}$ and PM_{10} outside the cave decreased from June 2015 to October, and then increased until January 2016, and the concentration of water-soluble ions showed an increasing trend from January to March 2016. The monthly distributions of Cl^-, SO_4^{2-}, NO_3^-, Na^+, K^+, Mg^{2+}, and Ca^{2+} outside the cave were similar to those inside the cave. F^- changed from January to March 2016, NH_4^+ concentration is high from October 2015 to March 2016. Both inside and outside of the cave, the ion mass loss is the lowest in September and the highest is in January or March.

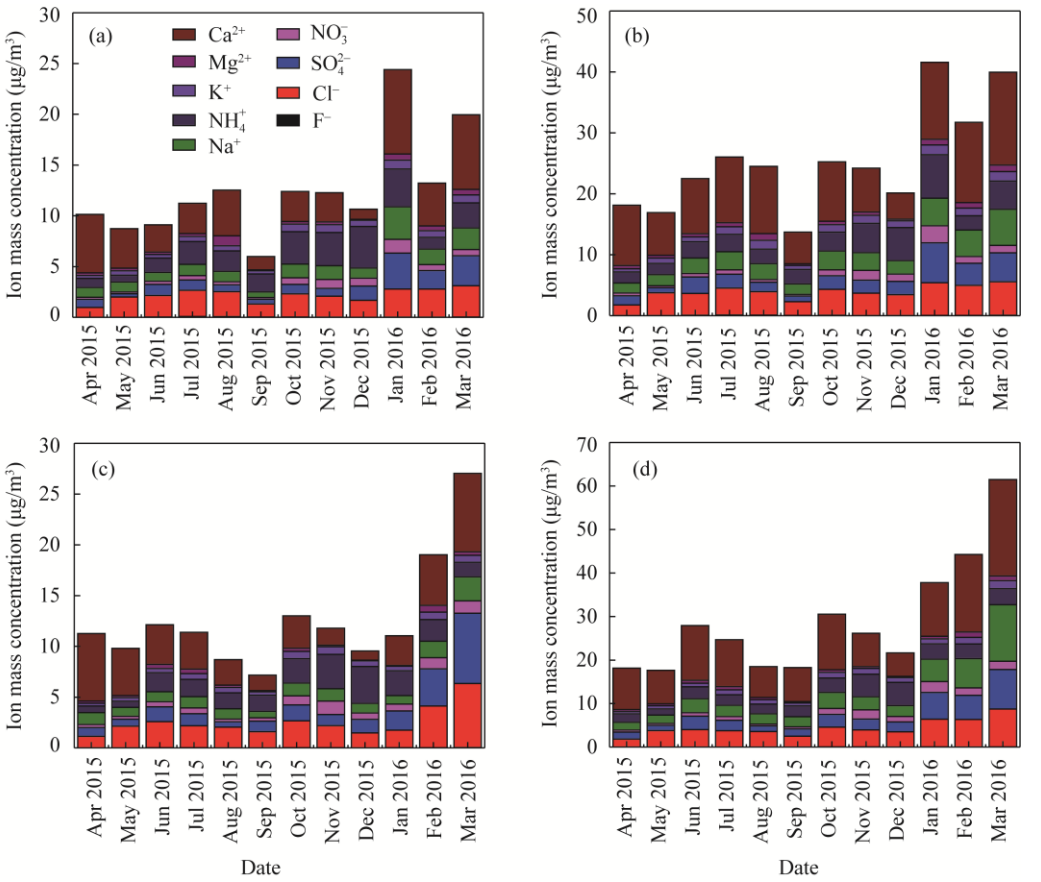

Fig. 5 Monthly average concentrations of water-soluble ions in $PM_{2.5}$ (a) and PM_{10} (b) inside and outside (c and d) the cave

3.3 Air particulate and water-soluble ions in particles of different sizes inside and outside the cave in extreme conditions

3.3.1 Influence of sandstorm and precipitation on atmospheric particulate matter

A sandstorm occurred in Dunhuang from 01:00 (LST) to 19:40 on 29 April, 2015, with a wind speed of 7.83 m/s at the top of the cave, and reached a maximum instantaneous wind speed of 12.72 m/s at 15:40. During the sandstorm, the wind direction varied from 0.0 ° to 355.2 °, and the main wind direction was NNE (north-north-east), which is conducive to the movement of pollutants into the cave. There was continuous precipitation from 17:30 to 21:10 on 29 April, and the cumulative precipitation reached 2.3 mm, accounting for 17.04% of the total precipitation in 2015, and the relative humidity reached 84.56%. Therefore, samples were collected to analyze the effects of special weather on the concentration of atmospheric particulates and water-soluble ions at the two sampling points in the Mogao Grottoes.

Figure 6 shows that during sunny weather, the concentrations of $PM_{2.5}$ and PM_{10} inside and outside the cave were 83.3333 and 270.8333, and 64.8148 and 170.8333 μg/m^3, and the concentrations of $PM_{2.5}$ and PM_{10} outside the cave were 0.78 and 0.63 times of the corresponding particle size concentration inside the cave. During precipitation period, the concentrations of $PM_{2.5}$ and PM_{10} inside and outside of the cave were 55.5556 and 95.8333, and 18.5185 and 24.5370 μg/m^3, and the concentrations of $PM_{2.5}$ and PM_{10} outside the cave was 0.33 and 0.26 times of that inside the cave, respectively. During sandstorm, the concentrations of $PM_{2.5}$ and PM_{10} inside and outside the cave were 287.6157, 367.2535, 474.5370, and 547.9167 μg/m^3, which were 3.45, 1.36, 7.32 and 3.21 times of those in the sunny weather, 5.18, 3.83, 25.63, and

22.33 times of those during precipitation period. And the concentrations of $PM_{2.5}$ and PM_{10} outside the cave were 1.65 and 1.49 times of the corresponding particle size concentration inside the cave. Sandstorm and precipitation affected the concentration of atmospheric particulates rapidly at the two monitoring points, especially the concentration of pollutants outside the cave.

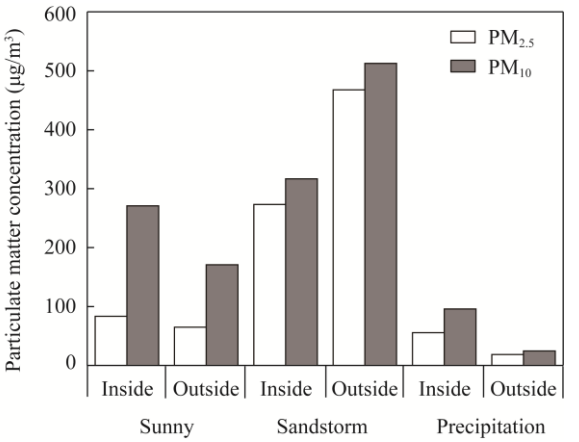

Fig. 6 Concentration of $PM_{2.5}$ and PM_{10} inside and outside the cave of the Mogao Grottoes under sunny weather, sandstorm weather, and precipitation

3.3.2 Influence of sandstorm and precipitation on water-soluble ions

Water-soluble ion concentration in $PM_{2.5}$ and PM_{10} were different inside and outside the cave (Fig. 7). On sunny days, the total concentrations of Cl^-, SO_4^{2-}, Na^+, NH_4^+, and Ca^{2+} in $PM_{2.5}$ and PM_{10}

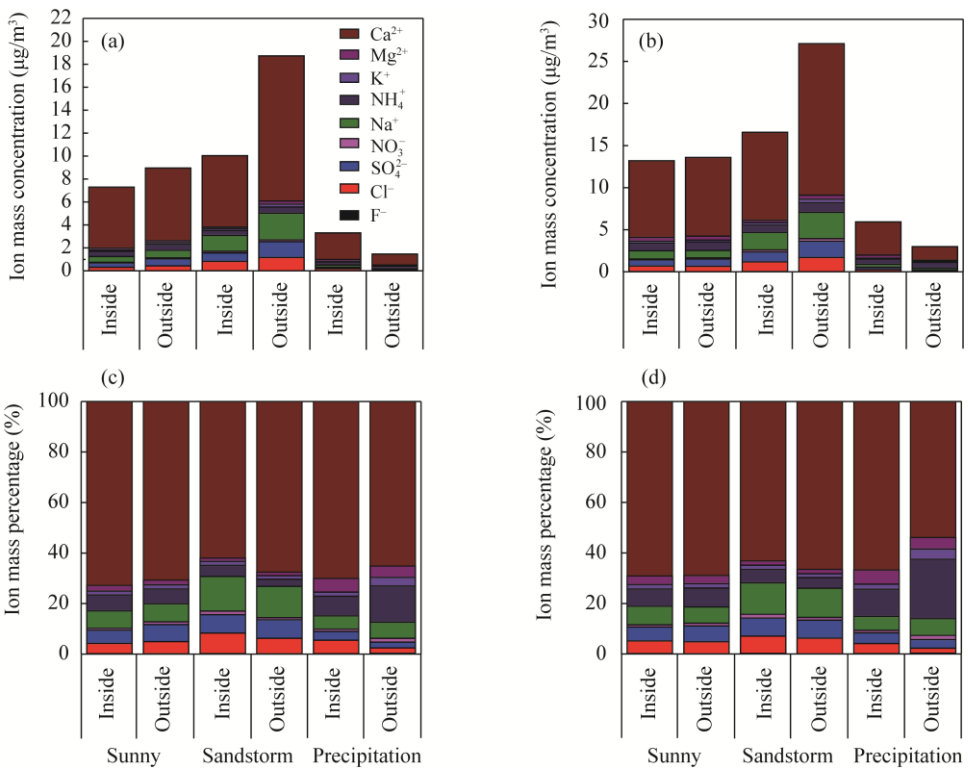

Fig. 7 Concentrations of water-soluble ions in $PM_{2.5}$ (a) and PM_{10} (b), relative proportion of soluble ions in $PM_{2.5}$ (c) and PM_{10} (d) inside and outside the cave of the Mogao Grottoes under sunny weather, sandstorm weather, and precipitation

inside and outside the cave were 6.9426, 12.3699, 8.5362, and 12.7496 μg/m^3, which accounted for 95.24%, 93.80%, 95.28%, and 93.88% of the total water-soluble ions, respectively. The total mass concentrations of other ions (F^-, NO_3^-, K^+ and Mg^{2+}) were 0.3469, 0.8180, 0.4225, and 0.8311 μg/m^3, accounting for only 4.76%, 6.20%, 4.72%, and 6.12%, respectively.

During the sandstorm, the total concentrations of Cl^-, SO_4^{2-}, Na^+, NH_4^+, and Ca^{2+} in $PM_{2.5}$ and PM_{10} inside and outside the cave were 9.5812, 15.7339, 18.0314, and 25.8900 μg/m^3, accounting for 95.51%, 94.91%, 96.28%, and 95.51% of the total water-soluble ions, respectively. The total mass concentrations of other ions (F^-, NO_3^-, K^+, and Mg^{2+}) were 0.4502, 0.8434, 0.6971 and 1.2170 μg/m^3, accounting for only 4.49%, 5.09%, 3.72%, and 4.49%, respectively.

During the precipitation period, the total concentrations of Cl^-, SO_4^{2-}, Na^+, NH_4^+, and Ca^{2+} in $PM_{2.5}$ and PM_{10} inside and outside the cave were 3.0384, 5.4094, 1.3198, and 2.6671 μg/m^3, the proportions to the total water-soluble ions were 91.89%, 91.25%, 90.31%, and 89.39%, and the total mass concentrations of other ions (F^-, NO_3^-, K^+, and Mg^{2+}) were 0.2681, 0.5188, 0.1416, and 0.3166 μg/m^3, accounting for only 8.11%, 8.75%, 9.69%, and 10.61%, respectively.

Further analysis of the data showed that under the influence of dust weather, the concentrations of Cl^-, SO_4^{2-}, NO_3^-, and Na^+ were 1.72–2.75, 1.63–2.29, 1.54–2.41, and 2.12–3.62 times of those on sunny days, and the proportion increased significantly. Concentrations of F^-, NH_4^+, K^+, Mg^{2+}, and Ca^{2+} changed little. While the proportions of NH_4^+, K^+, Mg^{2+}, and Ca^{2+} decreased, the proportion of F^- in the cave increased, and the proportion outside the cave decreased. Cl^- and Na^+ varied the most. The concentrations of Cl^-, SO_4^{2-}, Na^+, and Ca^{2+} during the sandstorm period were 4.65–36.51, 4.73–41.91, 6.30–24.87, and 2.65–13.28 times of those during precipitation period. The proportions of Cl^-, SO_4^{2-}, and Na^+ decreased significantly, and Ca^{2+} proportion increased in the cave and decreased outside the cave.

3.3.3 Backward trajectory of air flow

To identify potential transport pathways and possible source regions of the aerosols over the Mogao Grottoes, we used Hybrid Single-Particle Lagrangian Integrated Trajectory (HYSPLIT) model (http://ready.arl.noaa.gov/HYSPLIT_traj.php) to simulate the transport of sand and dust, and calculated a 24-h backward trajectory (Fig. 8). Heights of 500, 1000, and 1500 m were selected, and the back calculation time was 17:00 (UTC) on 28 April and 01:00 (LST) on 29 April, 2015. Combined with the ion concentrations listed in Figure 7, air masses arriving at the sampling site were classified into two types: (1) air masses that arrived on 29 April, which originated from or were transported through the arid regions of Hami City, Xinjiang Uygur Autonomous Region of China, through the Taklimakan Desert; and (2) through the Kumtag Desert to arrive at the sampling site, which may have resulted in the input of desert dust and some anthropogenic pollution. Thus, the concentrations of Cl^-, SO_4^{2-}, Na^+, NH_4^+, and Ca^{2+} were very high.

3.4 Acidity and alkalinity of atmospheric particles

Acidity of atmospheric particles can be determined by analyzing the balance of the main anion and cation charges in the particles (Zhou et al., 2016):

$$AE=c(Cl^-)/35.5+c(NO_3^-)/62+c(SO_4^{2-})/48+c(F^-)/19, \quad (1)$$

$$CE=c(NH_4^+)/18+c(Mg^{2+})/12+c(K^+)/39+c(Ca^{2+})/20+c(Na^+)/23, \quad (2)$$

where c is the concentration of each ion (μg/m^3); AE is the anion equivalent (μeq/m^3); and CE is the cation equivalent (μeq/m^3).

Figure 9 shows the fitting lines for equivalent values of cations to those of anions in $PM_{2.5}$ and PM_{10}, the slopes of the anion and cation balance of $PM_{2.5}$ and PM_{10} inside and outside the cave were greater than 1, i.e., 3.48, 6.06, 1.90, and 6.49, respectively. The results showed anion deficiency and alkalinity in the Mogao Grottoes.

3.5 Source analysis of water-soluble ions

The results of principal component analysis and orthogonal rotation factor load matrix are shown in Tables 3 and 4. As shown in Table 3, $PM_{2.5}$ in the cave contributed 76.22%. Factor 1 was loaded with Na^+, K^+, Cl^-, NO_3^-, and SO_4^{2-} and accounted for 40.73% of the total variance.

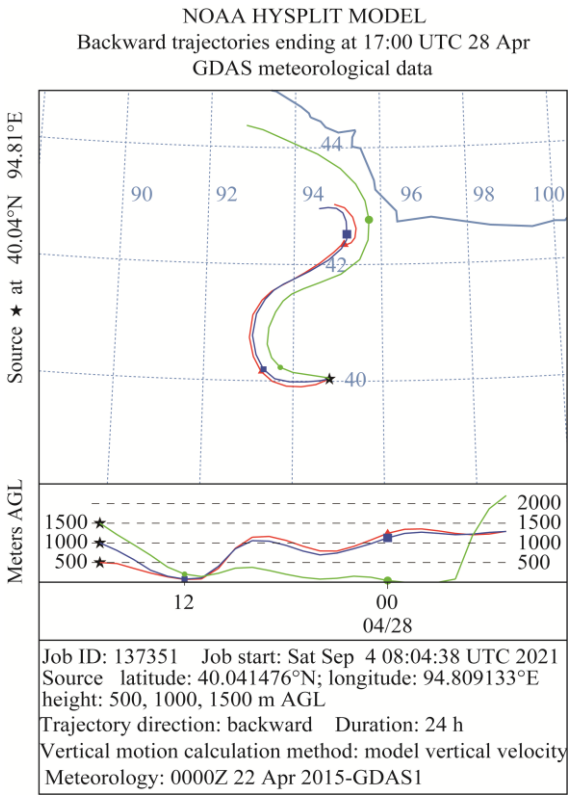

Fig. 8 Twenty-four-hour backward trajectory on 29 April, 2015. NOAA, National Oceanic and Atmospheric Administration; HYSPLIT, Hybrid Single-Particle Lagrangian Integrated Trajectory. GDAS, Global Data Assimilation System AGL, above ground level.

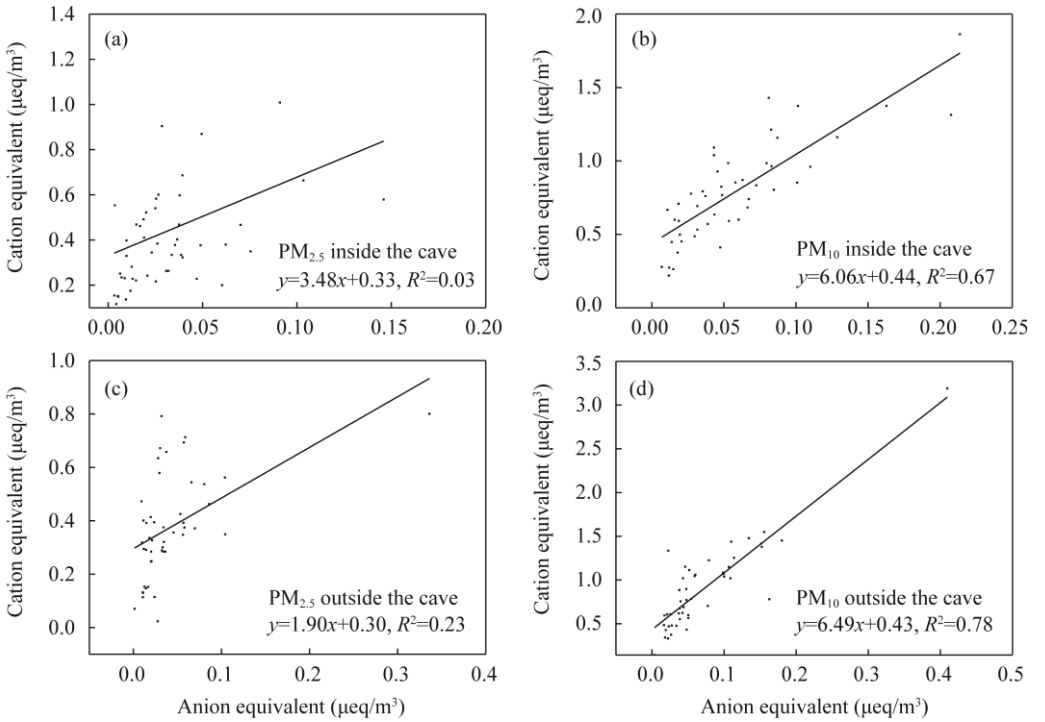

Fig. 9 Ion balance of $PM_{2.5}$ (a and c) and PM_{10} (b and d) inside and outside the cave of the Mogao Grottoes

Factor 2 was dominated by Mg^{2+} and Ca^{2+}. Factor 3 was dominated by F^-. In the cave (Table 4), the contribution rate of the three factors was 84.57% to the PM_{10}. The predominance of NH_4^+, K^+, NO_3^-, and SO_4^{2-} in factor 1 accounted for 33.89%. Na^+, K^+, F^-, and Cl^- in factor 2 had significant effects. Factor 3 had significant effects on Mg^{2+} and Ca^{2+}. In $PM_{2.5}$ outside the cave (Table 3), the contribution rate of the three factors was 82.90%. Factor 1 dominated by F^-, Cl^-, NO_3^-, and SO_4^{2-} had significant effects and accounted for 33.89%. In factor 2, Na^+, K^+, Mg^{2+}, and Ca^{2+} had significant effects. In factor 3, F^- has a significant effect. In PM_{10} outside the cave (Table 4), the contribution rate of the three factors was 88.28%. In Factor 1, Na^+, K^+, Mg^{2+}, Ca^{2+}, Cl^-, and SO_4^{2-} had significant effects and accounted for 51.27%. In Factor 2, NH_4^+ and NO_3^- had significant effects. F^- in factor 3 had significant effects.

Table 3 Varimax rotated factor loading matrix for water-soluble ions in $PM_{2.5}$ inside and outside the cave

Content	Load (inside the cave)			Load (outside the cave)		
	F_1	F_2	F_3	F_1	F_2	F_3
Na^+	0.805	0.287	–0.348	0.329	0.896	0.094
NH_4^+	0.563	–0.305	–0.472	0.070	–0.133	0.945
K^+	0.865	0.008	0.010	0.382	0.606	0.639
Mg^{2+}	–0.045	0.866	0.303	0.361	0.605	0.149
Ca^{2+}	0.144	0.962	–0.028	0.114	0.880	–0.359
F^-	0.113	0.306	0.764	0.823	0.118	0.153
Cl^-	0.705	0.283	0.260	0.771	0.498	0.060
NO_3^-	0.894	–0.084	0.221	0.794	0.238	0.407
SO_4^{2-}	0.787	0.001	0.157	0.863	0.315	–0.101
Eigenvalue	3.665	2.032	1.162	3.050	2.746	1.665
Contribution rate (%)	40.730	22.580	12.910	33.890	30.520	18.500

Table 4 Varimax rotated factor loading matrix for water-soluble ions in PM_{10} inside and outside the cave

Content	Load (inside the cave)			Load (outside the cave)		
	F_1	F_2	F_3	F_1	F_2	F_3
Na^+	0.511	0.727	0.135	0.878	0.292	0.183
NH_4^+	0.929	–0.057	0.020	0.071	0.846	0.415
K^+	0.673	0.603	0.146	0.729	0.536	0.224
Mg^{2+}	0.028	0.046	0.989	0.835	0.131	0.379
Ca^{2+}	0.060	0.350	0.911	0.902	0.009	0.268
F^-	–0.034	0.753	0.219	0.292	0.347	0.856
Cl^-	0.397	0.830	0.129	0.853	0.435	0.045
NO_3^-	0.868	0.319	0.012	0.485	0.743	0.096
SO_4^{2-}	0.745	0.519	0.032	0.864	0.378	0.077
Eigenvalue	3.050	2.647	1.914	4.614	2.110	1.222
Contribution rate (%)	33.890	29.420	21.260	51.270	23.440	13.580

4 Discussion

4.1 Effects of climatic factors and visitors

In addition to pollution sources, concentration of atmospheric particulate matter is affected by meteorological elements such as temperature, air pressure, wind speed, and precipitation (Guan et al., 2019; Vidal et al., 2019). Precipitation is considered to be a major factor in the long-term

preservation of murals (Wang et al., 2018). When the relative humidity exceeds 75%, it will increase the frequency of mural cracks and also influences the process of material transformation (Ogura et al., 2021). In Figure 3, difference between concentrations of $PM_{2.5}$ inside and outside the cave in our study (March) was much higher than that reported by Li et al. (2014) in the Pottery Depot of the Terra-cotta Warriors and Horses Museum of Qin Shihuang (inside, 76.1 μg/m^3; outside, 153.9 μg/m^3), and by Deng et al. (2022) in the Jinsha Site Museum (inside, 33.3 μg/m^3; outside, 39.4 μg/m^3), the difference of the result can be attributed to the windy and sandy weather in the arid environment of northern China. The cold air activity is more frequent and likely to cause sand and dust in the spring (from March to May) in Dunhuang. Mingsha Mountain that provides a sufficient sand source for windy weather is 1 km from the top of the Mogao Grottoes, although a shelterbelt locates directly in front of the Mogao Grottoes and provides protection against the sand and dust processes of the Mogao Grottoes (Xu et al., 2020).

The concentration of $PM_{2.5}$ and PM_{10} in the cave is also affected by the number of tourists in the peak tourist season in June–September 2015. In Table 1, the large temperature difference between outside and inside the cave is conducive to the migration of atmospheric particles. The higher the temperature, the stronger the airflow activity and the easier the diffusion of pollutants. When the relative humidity inside the cave is high, the particles are easily adsorbed on the surface of water vapor, which forms wet deposition, and then settles to the ground (Wang and Ogawa, 2015), thus reducing the concentration of suspended particles in the air. Precipitation in summer and autumn has a strong scavenging effect on pollutants (Tai et al., 2010). Concentration of particulate matter outside the cave is more likely to be affected by precipitation, as increase in humidity in the cave may cause the occurrence of salt damage to the murals. During the period of no air pollution, opening the cave door and increasing the air circulation plays an important role in reducing the concentration of suspended particulate matter in the air of the cave. Under high pressure, particulate matter does not readily diffuse, which easily causes $PM_{2.5}$ and PM_{10} to accumulate (Plocoste, 2022). High wind speed is conducive to the migration of particulate matter in the air. The main reason may be the abundant deposits in the Mingsha Mountain and the gravel Gobi area at the top of the cave. The average annual wind speed at the top of the cave is 4.23 m/s, and the frequency of sand-blowing wind (5 m/s, 2 m height) is as high as 69.80%. Higher wind speed can easily blow the pollutants deposited on the sand dunes in the Gobi area into the cave (Tan et al., 2016). The westerly wind (strong with the low frequency) is harmful to the murals due to sand transportation and accumulation in front of the cave (Li et al., 2012). The topography of the valley between the Sand Mountain and Sanwei Mountain to the east is not conducive to the diffusion of pollutants. The average annual wind speed in the cave is 0.54 m/s, and the frequency of sand blowing is only 0.01%, which is not conducive to pollution. The higher the wind speed is, the easier the particles infiltrate into the caves from the cracks of Cave 16, increasing the mass concentration of particles in the cave. On the other hand, the disturbance of tourists causes the secondary suspension of particles.

4.2 Sources of $PM_{2.5}$ and PM_{10}

Studies have found that soil in the top 50 cm in the Gobi area has high salinity (4.4% on average), and mainly consists of Na_2SO_4 and NaCl (Li et al., 2017). As shown in Table 2, salt content of the Gobi area in the Mogao Grottoes may affect the content of inorganic ions (Na^+, Cl^-, and SO_4^{2-}) in atmospheric particulates, and effective control of unstable surface that is prone to dust can reduce the sources of harmful salt ions in the murals. The concentration of NH_4^+ in the fine particles inside the cave was relatively high. The easier it is for fine particles to enter the fresco cracks, the greater the contribution of enriched salt ions to the mural degradation. Therefore, when removing dust on the surface of pigmented layer, more attention should be paid to the removal of fine particles. NO_3^- and SO_4^{2-} mainly comes from secondary pollution, such as coal combustion and soil dust in the surrounding rural areas, NO_3^-/SO_4^{2-} can distinguish mobile pollution sources and fixed pollution sources (Yao et al., 2002). In this study, NO_3^-/SO_4^{2-} in $PM_{2.5}$ and PM_{10} inside and outside the cave was less than 1, suggesting that coal combustion or dust contributes more

pollutants to the Mogao Grottoes than mobile source pollution. This is because motor vehicles are strictly prohibited in key protected areas, and tourist shuttle bus parks in an open area more than 200 m away from the cave, and buffering effect of protective forest belt in front of the cave effectively reduces the emission of secondary pollutants. This result is consistent with Yang et al. (2021), who found the significant impact of tourist visiting patterns on water-soluble ions in the Mogao Grottoes. In Figure 5a and b, May–August 2015 is the peak tourist season for the Mogao Grottoes, and tourists at this time account for more than 80% of the annual total. Mg^{2+} and Ca^{2+} may come from building sites and/or soil dust and dust weather in northern China (Li et al., 2015b), coal burning for heating, dust and pollutants from bare ground in winter, leading to increasing concentrations of Cl^-, SO_4^{2-}, Na^+, K^+, Mg^{2+}, and Ca^{2+}. K^+ is an important indicator of dust and biomass burning (Li et al., 2003), the concentration of K^+ was also relatively high from October to December 2015, and mainly derived from the burning of crop stalks such as corn and cotton in rural areas of Dunhuang. F^- mainly comes from ceramics, coal burning, and so on (Chen et al., 2013), the concentration of F^- was higher in July–August 2015, which may be mainly affected by the secondary suspension of particles containing coal combustion products caused by disturbance from tourists. The high concentration of NO_3^- from November 2015 to January 2016 may be related to the burning of coal in rural areas of Dunhuang for heating as well as sandy weather. The high concentration of NH_4^+ from October 2015 to January 2016 was mainly related to the burning of coal in rural areas of Dunhuang. In Figure 5c and d, it may be that the lack of wind and more rainfall in June–September reduced water-soluble ions concentration outside the cave. In January–March 2016, cold winter air contained fugitive dust from bare ground pollutants and rural heating coal, impacted the water-soluble ions. F^- occurred from January to March 2016, may be mainly affected by the long-distance transmission of crop straw combustion products (Chen et al., 2013). The high concentration of NH_4^+ from October 2015 to March 2016 was mainly related to the burning of coal for heating in the rural areas of Dunhuang. The content and type of water-soluble ions in the semi-closed caves are mainly affected by air exchange and tourist activities, while those outside the caves are mainly affected by natural environment. Therefore, in the period of frequent sandstorms, numerous tourists and vehicles, intensive crop burning and coal heating, the air exchange inside and outside the cave can be reduced by replacing the existing cave door. When the pollutant level is high, the internal air purification equipment and other measures can effectively reduce the concentration of water-soluble ions inside the cave.

4.3 Change of water-soluble ion in relation to dust storm

Change of particulate and water soluble ions is closely related to the extreme process of sand and duststorm in this area. Some research has shown that the concentration of particles, especially PM_{10}, during duststorm is much higher than that during non-duststorm (Guan et al., 2017), and chemical elements inside a cave are affected by weather conditions outside the cave (Whittlestone et al., 2003), including precipitation, clear or cloudy conditions and wind. Furthermore, the physical force generated by the large sand particles during a strong duststorm causes scratches on the surface of murals (Ogura et al., 2021). This study found that duststorm and precipitation have greater impact on pollutants inside and outside of the cave. That is why closing the cave and stopping visitors from visiting reduce the transmission of pollutants from outside to inside the cave. The effects of duststorm and precipitation on water-soluble ions are similar to those of Xu et al. (2020) and He et al. (2020). The sand and saline soil in the area deposited by the Daquan River, Kumtag Desert and Gobi area, and redistributed by wind influenced the water-soluble ions in atmospheric particles (Zhang et al., 2007).

Disruption and blistering of murals were mainly caused by NaCl and Na_2SO_4 (Jin et al., 2016). If particulate matter containing a large amount of Na^+, Cl^-, and SO_4^{2-} is deposited on or attached to wall paintings, and the humidity in the cave reaches more than 65%, the salt in the ground and the murals will be activated, resulting in the dissolution and crystallization of soluble salts and accelerating mural damage, such as blistering (Demas et al., 2015; Li et al., 2015a). During the

duststorm, the air mass mainly originated from the Hami area of Xinjiang, and was transported to the Dunhuang through the Taklimakan Desert and Kumtag Desert. This process may cause long-distance transport of atmospheric particles or short-distance local dust formation in the surrounding deserts and Gobi area. Therefore, during duststorm and sudden heavy rainfall, we recommend closing the caves to reduce the inward transmission of pollutants and humid air. At the same time, after duststorm, the dust accumulation in the caves and on the doors, windows, floors, and other areas should be cleaned up in time. The results of this study can be used as a reference for the improvement of early warning system of duststorm environment in the Mogao Grottoes and the decision-making of opening of the cave in response to extreme weather in advance. Deposition of alkaline or acidic particles on the relics will cause potential or immediate acid and salt corrosion of the surface and the color in a high-humidity environment (Mašková et al., 2017). In this study, the results showed alkalinity in the Mogao Grottoes, consistent with those at the Jinsha Site Museum (Deng et al., 2022), but contrary to the results of the Hanyang Tomb (Jia et al., 2015). The climate of Dunhuang is extremely arid, with low precipitation and high evaporation, and the salinity stays on the surface as evaporated groundwater makes the soil alkaline. There are no industrial pollution sources in the protected area. The alkalinity of atmospheric particulate matter in the Mogao Grottoes may be related to factors such as more crustal elements present in the cave and low levels of car exhaust pollution.

Water-soluble ion pollution has complex origins comprising sea fog emissions, soil dust, biomass combustion, and fossil fuel combustion emissions (Wang, 2005). In Tables 3 and 4, Na^+ and Cl^- may come from Gobi area and the Daquan River, and NH_4^+ is mainly derived from secondary pollution sources such as rural coal combustion. K^+ derived mainly from the crop straw burning. In summary, the pollution sources of atmospheric particulates of different particle sizes in the Mogao Grottoes are diverse and include mainly straw burning, secondary pollution sources, soil dust, dry spring rivers, and from tourist activities. Therefore, it is necessary to strengthen the control of the burning of agricultural crops in Dunhuang, reduce the operation of motor vehicles (especially private cars of employees) in protection zone of the Mogao Grottoes, increase the popularization of new energy commuter vehicles, and reduce the cracking sand hills and dry springs on the top of the caves.

5 Conclusions

Concentrations of $PM_{2.5}$ and PM_{10} inside and outside the cave were the highest in March 2016 and the lowest in December 2015. The lower particulate matter concentration from June to September is associated with good diffusion conditions and increased precipitation and reduced wind impact. Ca^{2+}, NH_4^+, Na^+, Cl^-, and SO_4^{2-} were main components. There was a consistent relationship of $PM_{2.5}$ and PM_{10} between the inside and outside of the cave, and the particulate source was mainly coal combustion or dust from the ground, which contributed more pollutants in the Mogao Grottoes, with less mobile source pollution. Duststorm can lead to sharp increases in the air particulate concentration and can cause predictable deterioration of mural covers. The control of atmospheric particulate matter pollution in the Mogao Grottoes should be based on improving the comprehensive system of wind and sand prevention and control, limiting the number of tourists, adjusting and opening the caves, and cleaning the ground of sand or dust deposits in a time, as well as adding effective ventilation and air purification and other intelligent control systems.

Acknowledgements

This work was supported by the National Natural Science Foundation of China (51962001, 32260292), the National Key Research & Development Projects (2020YFC1522200), and the Gansu Provincial Science and Technology Plan Project (20JR5RA051, 21YF1FF371). The authors also thank the anonymous reviewers and the editor who helped to improve the quality of this paper.

References

Abbott A. 2010. Ancient Italian artefacts get the blues. Nature, 466: 306–307.

Agnew N. 2004. Conservation of ancient sites on the Silk Road. In: Agnew N. The 2nd International Conference on the Conservation of Grotto Sites, Mogao Grottoes, Dunhuang. Los Angeles: Getty Publications, 3–30.

Bouchlaghem K, Nsom B, Latrache N, et al. 2009. Impact of Saharan dust on PM_{10} concentration in the Mediterranean Tunisian coasts. Atmospheric Research, 92(4): 531–539.

Brimblecombe P. 1990. The composition of museum atmospheres. Atmospheric Environment Part B Urban Atmosphere, 24(1): 1–8.

Broughton L. 1875. Report of commission on the site for a new National Gallery. In: Broughton L. British Sessional Papers. London: House of Commons, 2: 24.

Cao J J, Rong B, Lee S C, et al. 2005. Composition of indoor aerosols at Emperor Qin's Terra-cotta Museum, Xi'an, China, during summer. China Particuology, 3(3): 170–175.

Chatoutsidou S E, Maskova L, Ondrackova L, et al. 2015. Modeling of the aerosol infiltration characteristics in a cultural heritage building: The baroque library hall in prague. Building and Environment, 89: 253–263.

Chen B, Stein A F, Maldonado P G, et al. 2013. Size distribution and concentrations of heavy metals in atmospheric aerosols originating from industrial emissions as predicted by the HYSPLIT model. Atmospheric Environment, 71: 234–244.

Demas M, Agnew N, Fan J. 2015. Strategies for Sustainable Tourism at the Mogao Grottoes of Dunhuang, China. Dordrecht: Springer, 1–114.

Deng J L, Jiang L M, Miao W W, et al. 2022. Characteristics of fine particulate matter ($PM_{2.5}$) at Jinsha Site Museum, Chengdu, China. Environmental Science and Pollution Research, 29(1): 1173–1183.

Fan J. 2000. The conservation and management of the Mogao Grottoes, Dunhuang. Dunhuang Research, 63(1): 1–4. (in Chinese)

Ghedini N, Gobbi G, Sabbioni C, et al. 2000. Determination of elemental and organic carbon on damaged stone monuments. Atmospheric Environment, 34 (25): 4383–4391.

Ghedini N, Ozga I, Bonazza A, et al. 2011. Atmospheric aerosol monitoring as a strategy for the preventive conservation of urban monumental heritage: The Florence Baptistery. Atmospheric Environment, 45(33): 5979–5987.

Guan Q, Cai A, Wang F, et al. 2017. Spatio-temporal variability of particulate matter in the key part of Gansu Province, western China. Environmental Pollution, 230: 189–198.

Guan Q Y, Luo H P, Pan N H, et al. 2019. Contribution of dust in northern China to PM_{10} concentrations over the Hexi Corridor. Science of the Total Environment, 660(10): 947–958.

Hanapia N, Din S A M. 2012. A study on the airborne particulates matter in selected museums of Peninsular Malaysia. Procedia–Social and Behavioral Sciences, 50: 602–613.

He D P, Wu F S, Xu R H, et al. 2020. Characteristics of atmospheric particulates and organic carbon in Dunhuang Mogao Grottoes. Journal of Lanzhou Jiaotong University, 39(6): 92–98. (in Chinese)

Hu T F, Lee S C, Cao J J, et al. 2009. Characterization of winter airborne particles at Emperor Qin's Terra-cotta Museum, China. Science of the Total Environment, 407(20): 5319–5327.

Jia W T, Hu T F, Cao J J, et al. 2015. Characterization of microclimate and aerosol inside the Display Hall of Burial Pits at the Hanyangling Museum. Journal of Earth Environment, 6(5): 307–316. (in Chinese)

Jin Z L, Chen G Q, Xia Y, et al. 2015. Comparative study of salt damage caused by sulfates and chlorides to mural paintings-evidence of superpenetration, migration and crystallization destruction resulting from sodium sulfate. Sciences of Conservation and Archaeology, 7(1): 29–38. (in Chinese)

Li C L, Yan F P, Kang S C, et al. 2016. Concentration, sources, and flux of dissolved organic carbon of precipitation at Lhasa City, the Tibetan Plateau. Environmental Science and Pollution Research, 23(13): 12915–12921.

Li G S, Qu J J, Wang W F, et al. 2012. Overall efficiency of a V shaped nylon net fence in preventing sand damage to the Mogao Grottoes. Sciences in Cold and Arid Regions, 4(2): 163–174.

Li G S, Wang W F, Qu J J, et al. 2013. Study on temperature and humidity environment of grotto 72 at the Mogao Grottoes in Dunhuang, China. International Journal of Climatology, 33(8): 1863–1872.

Li H, Gao Y, Wang C, et al. 2014. Evaluation and analysis of air quality impact in the pottery storage-room of the Emperor Qin Shihuang's Mausoleum Site Museum. Sciences Conservation and Archaeology, 26(1): 34–41. (in Chinese)

Li H, Wang W, Zhan H, et al. 2017. Measurement and analysis of the yearly characteristics of deep-buried phreatic evaporation in a hyper-arid area. Acta Ecologica Sinica, 37(1): 53–59.

Li H, Hu T F, Du W S. 2019. Comparison of site environments of Emperor Qin's Terracotta Warriors and Horses Museum and Han Yangling Museum. Conservation of Cultural Relics and Archaeological Science, 31(2): 53–60. (in Chinese).

Li H S, Wang W F, Zhan H T, et al. 2015. Water in the Mogao Grottoes, China: Where it comes from and how it is driven. Journal of Arid Land, 7(1): 37–45.

Li J, Pósfai M, Hobbs P V, et al. 2003. Individual aerosol particles from biomass burning in southern Africa: 2, Compositions and aging of inorganic particles. Journal of Geophysical Research, 108(D13): 8484, doi:10.1029/2002JD002310.

Li L, An J Y, Zhou M, et al. 2015. Source apportionment of fine particles and its chemical components over the Yangtze River Delta, China during a heavy haze pollution episode. Atmospheric Environment, 123: 415–429.

Liu H L, Wang X D, Guo Q L, et al. 2020. Experimental investigation on the correlation between rainfall infiltration and the deterioration of wall paintings at Mogao Grottoes, China. Bulletin of Engineering Geology and the Environment, 79: 1199–1207.

Mašková L, Smolík J, Ďurovič M. 2017. Characterization of indoor air quality in different archives-possible implications for books and manuscripts. Building Environment, 120: 77–84.

Merello P, García-Diego F J, Zarzo M. 2014. Diagnosis of abnormal patterns in multivariate microclimate monitoring: A case study of an open-air archaeological site in Pompeii (Italy). Science of the Total Environment, 488–489: 14–25.

Mikayama A, Hokoi S, Ogura D. 2015. Effects of drifting sand particles on deterioration of mural paintings on the east wall of Cave 285 in Mogao Caves, Dunhuang. Energy Procedia, 78: 1311–1316.

Natarajan N, Vasudevan M, Dineshkumar S K, et al. 2022. Effects of air pollution on monumental buildings in India: An overview. Environmental Science and Pollution Research, 29(20): 29399–29408.

Ogura D, Hase T, Nakata Y, et al. 2021. Influence of environmental factors on deterioration of mural paintings in Mogao Cave 285, Dunhuang. Case Studies in Building Rehabilitation, 13: 105–159.

Pipal A S, Satsangi P G, Tiwari S, et al. 2014. Study of mineral aerosols in fine ($PM_{2.5}$) and coarse (PM_{10}) atmospheric particles over a world heritage site at Agra, India. Environmental Technology and Management, 17(6): 538–553.

Plocoste T. 2022. Multiscale analysis of the dynamic relationship between particulate matter (PM_{10}) and meteorological parameters using CEEMDAN: A focus on "Godzilla" African dust event. Atmospheric Pollution Research, 13(1): 101252, doi: 10.1016/j.apr.2021.101252.

Poulain L, Fahlbusch B, Spindler G, et al. 2021. Source apportionment and impact of long-range transport on carbonaceous aerosol particles in central Germany during HCCT-2010. Atmospheric Chemistry and Physics, 21(5): 3667–3684.

Sabbioni C, Ghedini N, Bonazza A. 2003. Organic anions in damage layers on monuments and buildings. Atmospheric Environment, 37(9–10): 1261–1269.

Sakka A, Gerasopoulos E, Liakakou E, et al. 2020. Spatial variability of aerosols over Greek archaeological sites using Space-Borne Remote Sensing. Journal of Cultural Heritage, 46: 207–217.

Singh R, Sharma B S. 2012. Composition, seasonal variation, and sources of PM_{10} from world heritage site Taj Mahal, Agra. Environmental Monitoring and Assessment, 184(10): 5945–5956.

Tai A, Mickley L J, Jacob D J. 2010. Correlations between fine particulate matter ($PM_{2.5}$) and meteorological variables in the United States: Implications for the sensitivity of $PM_{2.5}$ to climate change. Atmospheric Environment, 44(32): 3976–3984.

Tan L H, Zhang W M, Qu J J, et al. 2016. Aeolian sediment transport over Gobi: Field studies atop the Mogao Grottoes, China. Aeolian Research, 21: 53–60.

Tétreault J. 2003. Airborne Pollutants in Museums, Galleries and Archives: Risk Assessment, Control Strategies, and

Preservation Management. Ottawa: Canadian Conservation Institute, 1–168.

Uring P, Chabas A, Alfaro S. 2019. Dust deposition on textile and its evolution in indoor cultural heritage. The European Physical Journal Plus, 134(6): 1–9.

Vidal F, Vicente R, Silva J M. 2019. Review of environmental and air pollution impacts on built heritage: 10 questions on corrosion and soiling effects for urban intervention. Journal of Cultural Heritage, 37: 273–295.

Wang J H, Ogawa S. 2015. Effects of meteorological conditions on $PM_{2.5}$ concentrations in Nagasaki, Japan. International Journal of Environmental Research and Public Health, 12(8): 9089–9101.

Wang J L, Yan Z F, Wang X D, et al. 2016. Experimental research on mechanical ventilation system for Cave 328 in Mogao Grottoes, Dunhuang, China. Energy and Buildings, 130: 692–696.

Wang W F, Ma X, Ma Y T, et al. 2011. Molecular characterization of airborne fungi in caves of the Mogao Grottoes, Dunhuang, China. International Biodeterioration and Biodegradation, 65(5): 726–731.

Wang W F. 2018. Prevention and Control of Sand Dunes Hazard in Dunhuang Mogao Grottoes. Beijing: Science Press, 2–7. (in Chinese)

Wang X M, Carmichael G R, Chen D L, et al. 2005. Impacts of different emission sources on air quality during March 2001 in the Pearl River Delta (PRD) region. Atmospheric Environment, 39(29): 5227–5241.

Whittlestone S, James J, Barnes C. 2003. The relationship between local climate and radon concentrations in the Temple of Baal, Jenolan Caves, Australia. Helictite, 38: 39–44.

Xu R H, Wu F S, Wang W F, et al. 2020. Chemical elemental characteristics of atmospheric inhalable particulates in Dunhuang Mogao Grottoes. Arid Land Geograpuy, 43(5): 1231–1241. (in Chinese)

Yang X J, Wu F S, Xu R H, et al. 2021. Variation and source analysis of water-soluble ions in the atmospheric particles of Mogao Grottoes at Dunhuang. Plateau Meteorology, 40(2): 436–447. (in Chinese)

Yao X, Chan C K, Ming F, et al. 2002. The water-soluble ionic composition of $PM_{2.5}$ in Shanghai and Beijing, China. Atmospheric Environment, 36(26): 4223–4234.

Yao Y, He C, Li S, et al. 2019. Properties of particulate matter and gaseous pollutants in Shandong, China: Daily fluctuation, influencing factors, and spatiotemporal distribution. Science of the Total Environment, 660(2): 384–394.

Zhang E K, Cao J J, Wang X D, et al. 2007. A preliminary study of characterization of indoor and outdoor air quality in Dunhuang Mogao Grottoes. Journal of the Graduate School of the Chinese Academy of Sciences, 24(5): 612–618. (in Chinese)

Zhang G B, Wang W F, Xue P, et al. 2009. Comparative analysis of air exchange rate in typical caves of Mogao Grottoes in Dunhuang. Dunhuang Research, (6): 100–104. (in Chinese)

Zhang G B, Tan L H, Zhang W M, et al. 2022. Temporal variation of airborne dust concentrations in the Mogao Grottoes, Dunhuang, China. Frontiers in Environmental Science, 10: 878466, doi:10.3389/fenvs.2022.878466.

Zhou J B, Xing Z Y, Deng J J, et al. 2016. Characterizing and sourcing ambient $PM_{2.5}$ over key emission regions in China I: Water-soluble ions and carbonaceous fractions. Atmospheric Environment, 135: 20–30.